frontiers in Materials

ORIGINAL RESEARCH
published: 03 June 2021
doi: 10.3389/fmats.2021.534407

Mechanical Properties of WC-Si_3N_4 Composites With Ultrafine Porous Boron Nitride Nanofiber Additive

Ting Cao[1], Xiaoqiang Li[1], Jingmao Li[1], Yang Huang[2], Shengguan Qu[1], Chao Yang[1], Liang Liang[1] and Tao Song[2]*

[1] National Engineering Research Center of Near-Net-Shape Forming for Metallic Materials, South China University of Technology, Guangzhou, China, [2] School of Materials Science and Engineering, Hebei University of Technology, Tianjin, China

OPEN ACCESS

Edited by:
Suryanarayana Challapalli, University of Central Florida, United States

Reviewed by:
Mehdi Shahedi Asl, University of Mohaghegh Ardabili, Iran
Zhi Wang, South China University of Technology, China
Francesco Colangelo, University of Naples Parthenope, Italy
Pasquale Vena, Politecnico di Milano, Italy
Ehsan Ghasali, Materials and Energy Research Center, Iran

***Correspondence:**
Xiaoqiang Li
lixq@scut.edu.cn

Specialty section:
This article was submitted to Mechanics of Materials, a section of the journal Frontiers in Materials

Received: 14 February 2020
Accepted: 16 April 2021
Published: 03 June 2021

Citation:
Cao T, Li X, Li J, Huang Y, Qu S, Yang C, Liang L and Song T (2021) Mechanical Properties of WC-Si_3N_4 Composites With Ultrafine Porous Boron Nitride Nanofiber Additive. Front. Mater. 8:534407. doi: 10.3389/fmats.2021.534407

WC-10 wt.% Si_3N_4 composites toughened with ultrafine porous boron nitride nanofiber (0, 0.01, 0.05, 0.1, and 0.15 wt.%) were prepared for the first time by spark plasma sintering. Compared with the WC-Si_3N_4 composite sintered in the same condition, the obtained WC-10 wt.% Si_3N_4 composites with ultrafine porous boron nitride were found to possess better hardness and fracture toughness. In addition, the Si_3N_4 phase in the UPBNNF toughened composites did not exhibit traditional catastrophic fracture as indicated in most investigations. In this study, the phenomena are discussed, and a probable mechanism is elucidated. It is deduced that the approach could be extended to materials with a feature of internal liquid phase during the sintering process and could improve hardness and fracture toughness.

Keywords: porous nanofiber, WC, Si3N4, Young's modulus, fracture mode

INTRODUCTION

Tungsten carbide (WC) has numerous advantages, including high Young's modulus, high hardness, and excellent wear-resistance (Zhang et al., 2009; Kumar et al., 2011; Namini et al., 2019; Sakkaki et al., 2019; Fattahi et al., 2020a,b). However, the shortcoming of WC is brittleness. Therefore, most industrial WC-based materials are WC-Co composites, which are typically applied as cutting tools and molds (Chang et al., 2015; Norgren et al., 2015). Co is beneficial for improving fracture toughness because of its ductility and wettability to WC. In addition, binderless WC-based materials continue to be investigated due to their merits of corrosion-resistance and red hardness in comparison to binder-containing composites. In this manner, carbides are mostly used (e.g., VC, Cr_2C_3, TaC, and TiC (Kim et al., 2008; Poetschke et al., 2012; Nino et al., 2019). The toughening effects of oxides such as MgO, Al_2O_3, and ZrO_2 are also investigated on the WC matrix (El-Eskandarany, 2000, 2005; Basu et al., 2004; Zheng et al., 2012, 2013b).

Carbon (CNT) and boron nitride (BNNT) nanotubes have outstanding mechanical properties, which have attracted attention in materials reinforcement (Wang et al., 2011; Yadhukkulakrishnan et al., 2012; Tatarko et al., 2014; Vasudevan et al., 2016; Jin et al., 2017; Li et al., 2018). CNT with exceptionally high Young's modulus in the terapascal (TPa) range and tensile strength of as much as 60 GPa has been investigated as a toughening phase for a long time (Han et al., 2018). BNNT possesses high chemical stability in addition to previously mentioned advantages. However, difficulties remain in BNNT synthesis with large quantities and low costs (Golberg et al., 2007, 2010). As an alternative for environmental chemistry and hydrogen storage, Lin et al. (2016)

prepared an ultrafine porous boron nitride nanofiber (UPBNNF) with a high specific surface area of 515 m^2/g and a total pore volume of 0.566 cm^3/g using freeze-drying and pyrolysis processes. But studies on the toughening effect of the porous fiber are rare yet.

WC-Si_3N_4 composites have been considered in detail with respect to the sintering process, phase transformation, microstructure, and mechanical properties using spark plasma sintering (SPS) (Li et al., 2013; Zheng et al., 2013a, 2015). In this study, the WC-10 wt.% Si_3N_4 composites with addition of UPBNNF were prepared using SPS to investigate UPBNNF's effects on the overall mechanical properties. The mechanical phenomena after testing were discussed on experimental data and fracture theory.

EXPERIMENTAL PROCEDURE

For starting materials, we used WC (200 nm, purity > 99.9%, Xuzhou Jiechuang New Material Technology Co., Ltd., China), Si_3N_4 (∼1 μm, >95% α-phase, Xuzhou Jiechuang New Material Technology Co., Ltd., China), Y_2O_3 (5–10 μm, purity > 99.9%, Sinopharm Chemical Reagent Co., Ltd., China) and Al_2O_3 (∼1 μm, purity > 99.9%, Beijing Mountain Technological Development Center, China), UPBNNF (diameter: 20–60 nm, length: tens of micrometers; Boron Nitride Research Center, Hebei University of Technology, China). The WC-10 wt.% Si_3N_4 ($93Si_3N_4 + 6Y_2O_3 + 1Al_2O_3$, wt.%) powder mixtures with the addition of 0, 0.01, 0.05, 0.1, and 0.15 wt.% UPBNNF ultrasonically dispersed in ethanol in advance were wet-mixed on a planetary ball mill. Then they were dried, sieved, poured into a cylindrical graphite die, and heated to 1750°C (monitored by infrared thermometer) without soaking time under applied pressure of 30 MPa in ≤6 Pa vaccum. Other processing details have been shown in Li et al. (2013) and Zheng et al. (2013a, 2015). Thereafter, the five obtained WC–UPBNNF specimens were named 10S, 10S0.01B, 10S0.05B, 10S0.1B, and 10S0.15B, respectively, in terms of their UPBNNF content. For necessary supporting details, an over-sintering 10S0.1B specimen was prepared with the sintering parameters of 1750°C and 5-min soaking time.

The density of the specimens (Φ20 × 10 mm) was measured using water before being calculated by the Archimedes principle. The hardness (HV_{10}) was evaluated on a Vickers hardness tester (430SVA, Wilson Wolpert Co., Ltd., China) with a load of 10 kg. An indentation with a load of 30 kg was produced to illustrate crack details on the 10S0.05B specimen. The fracture toughness (K_{Ic}) was calculated based on the radial crack produced by Vickers indentation according to the Anstis formula (for half-penny crack):

$$K_{\mathrm{I}c} = 0.016 \times \left(\frac{E}{H}\right)^{\frac{1}{2}} \times \frac{P}{c^{3/2}},$$

where E is Young's modulus, H is hardness, P is peak load, and c is the characteristic dimension (Anstis et al., 1981). The reported values were the averages of the data obtained from five indentation tests. Using the pulse-echo overlap ultrasonic technique (ultrasonic generator CTS-32, SIUI, China; data collection system DPO5034, Tektronix, United States; longitudinal wave detector K 10K-52832, GE, United States; transverse wave detector MB2Y, KK, Germany), we determined the elastic modulus of all samples. Sound velocity is measured to inversely calculate Young's modulus, which is based on influence of intrinsic properties of materials like elastic properties on sound propagation. As a reference, the Young's modulus of specimens shown in **Table 1** was also calculated according to Voigt's formula (upper boundary):

$$E = \sum E_i V_i,$$

where E_i and V_i represent the Young's modulus and volume fraction of every phase, respectively (Meyors and Chawla, 1999).

Phase identification was conducted using an X-ray diffractometer (XRD, D8 Advance, Bruker Co., Germany) with Cu Kα radiation. The wt. fraction of the β phase in Si_3N_4 was calculated based on the α (200)/β (200) ratio of the diffraction peak heights (PH) based on the method reported by Pigeon and Varma (1992). The PH data were collected at a 0.02° $step^{-1}$ between 25 and 29° of 2theta (time constant 2 s) with the contribution subtracted due to background noise:

$$\alpha/\beta \text{ phase ratio} = 4.9381(\mathrm{PH}) + 0.1144(\mathrm{PH})^2 + 0.08106(\mathrm{PH})^3,$$

$$\text{wt. fraction} = 1/(1 + \alpha/\beta).$$

The microstructure as well as the Vickers indentations was examined using high-resolution scanning electron microscopy (HRSEM, Nova Nano 430, FEI, United States).

RESULTS AND DISCUSSION

The displacement of the lower punch, which reflects the densification process of the sample, and the temperature were automatically recorded during sintering. **Figure 1** shows shrinkage rate curves of the specimens heated to 1750°C without soaking time. As the shrinkage rate became positive, the powders were densified until the shrinkage rate was again reduced to zero. For the fine grain WC-10 wt.% Si_3N_4 and those specimens with the addition of UPBNNF, the densification process started at approximately 900°C. Much faster densification rates were observed for all specimens when the sintering temperature rose to 1400°C. Finally, the densification process ended at approximately 1600°C.

Figure 2 shows the XRD patterns of WC-10 wt.% Si_3N_4 with and without UPBNNF specimens. The wt. fraction of the β phase calculated from the XRD data in **Figure 3** are listed in **Table 1**. The specimens containing UPBNNF had a higher wt. fraction of the β phase than the specimens without the fiber. The microstructures of composites containing UPBNNF that can be seen in **Figure 4** are not different from the WC-10 wt.% Si_3N_4 reported in our previous works (Li et al., 2013; Zheng et al., 2013a, 2015). In the microscopy examination processes that we performed, UPBNNF was hardly

TABLE 1 | Characteristics of WC-Si_3N_4-UPBNNF specimens.

Specimen	Density (g/cm^3)	β-Si_3N_4 (100%)	Hardness (GPa)	Elasticity modulus (GPa, calculated)	Elasticity modulus (GPa, tested)	Fracture toughness (MPa·m$^{1/2}$)
10S	11.45	16.96	17.76 ± 0.25	572	521	7.70 ± 0.56
10S0.01B	11.39	20.44	18.32 ± 0.33	567	793	10.99 ± 0.41
10S0.05B	11.40	18.79	20.56 ± 0.87	556	779	10.57 ± 0.38
10S0.1B	11.41	27.51	19.04 ± 0.39	544	775	10.50 ± 0.68
10S0.15B	11.37	24.83	19.12 ± 0.56	532	755	10.09 ± 0.76

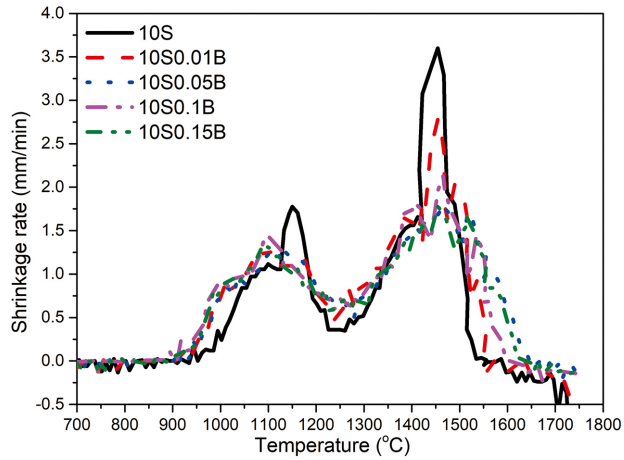

FIGURE 1 | Densification curves of the composite specimens.

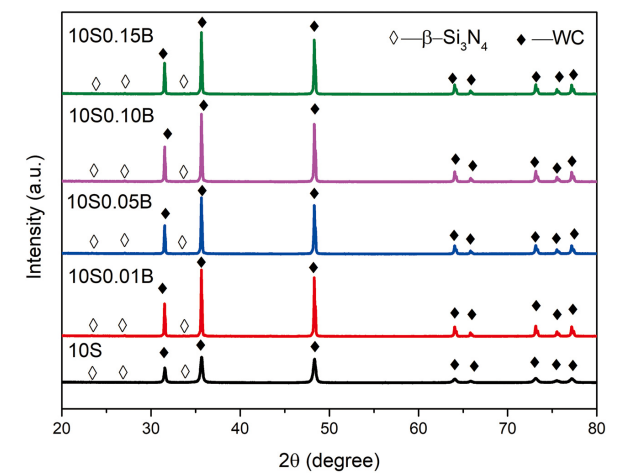

FIGURE 2 | XRD patterns of the composite specimens.

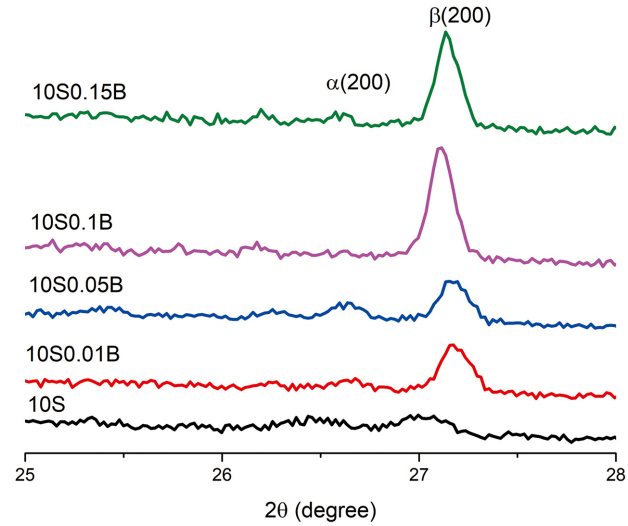

FIGURE 3 | XRD patterns for α-Si_3N_4 (100) and β-Si_3N_4 (200) crystal planes of the composite specimens.

to be observed, which could be attributed to the low contrast of BN in the composites.

Values for the hardness and fracture toughness of WC-10 wt.% Si_3N_4 with different ratios of UPBNNF composites are listed in **Table 1**. All specimens containing UPBNNF were better in terms of both hardness and fracture toughness as compared to the WC-10 wt.% Si_3N_4. **Table 1** also shows the tested Young's modulus values of specimens as well as the theoretical upper boundary calculated from Voigt's formula, and the UPBNNF-containing specimens had abnormally high values (the highest reached 793 GPa) that were superior to the value of pure WC (700 GPa), with nearly changeless density. If the calculated values are obtained based on tested value of 10S, the calculated values along with growth of UPBNNF additive amount are 520, 519, 518, and 517 GPa, respectively. The crack path details of all composites are presented in **Figure 5**, where tearing and scratch patterns on Si_3N_4 in the composites containing UPBNNF are visible. The crack pattern of Si_3N_4 grains in composites is different from the transgranular crack pattern of Si_3N_4 with clean edges. When the crack passes the Si_3N_4 grains in the composites, it appears healed, which is also unlike the traditional crack pattern of ceramic matrices. Under a 10-kg load, UPBNNF is rarely observed. Therefore, a 30-kg load is employed to produce a bigger crack. In the crack images of **Figure 6**, UPBNNF can be observed in the UPBNNF-containing specimens. In particular, single fibers can be seen between the broken parts of Si_3N_4.

In the aforementioned results, the fracture mode identified in the results can be noticeable. In general, Si_3N_4 ceramics are known for catastrophic fracture, and thorough fracture of Si_3N_4 grains with clean edge is observed (a fine image of fracture

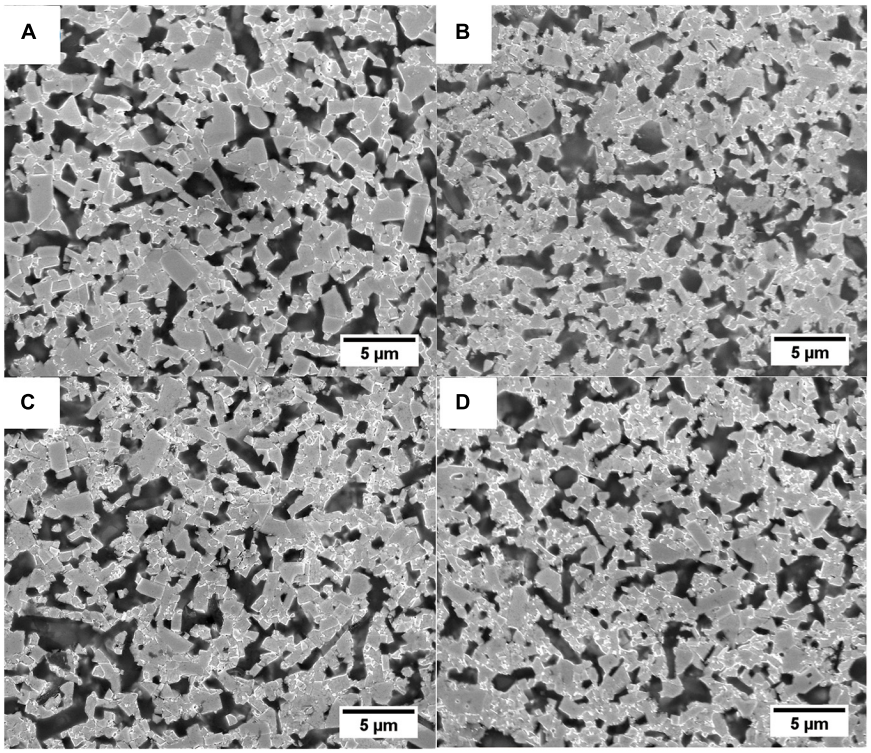

FIGURE 4 | SEM micrographs of the indentation crack paths in **(A)** 10S0.01B, **(B)** 10S0.05B, **(C)** 10S0.1B, and **(D)** 10S0.15B.

of Si_3N_4 grains is provided in Riley (2000), Ii et al. (2004), Klemm (2010), Zhou et al. (2014), and Hu et al. (2019). However, different cases of tears and scratches emerge on the Si_3N_4 grains in the composites with UPBNNF, as shown in **Figure 5**, which means fractures of Si_3N_4 occur partly under a given load. The phenomena has been barely observed in other Si_3N_4-containing composites. It can be deduced that the whole fracture process involves two steps at least during a given time interval under a limited load. Therefore, these crack patterns are not the traditional catastrophic fracture mode of Si_3N_4.

Theories on fracture and toughening can be simply divided two theoretical categories: the microstructural and the atomic. Fracture and toughening phenomena are usually elucidated by microstructure theory with respect to interface energy that is sufficient in most cases (Marshall and Evans, 1985; Becher et al., 1988; Becher, 1991). Furthermore, analysis on fracture is based on thermodynamics. According to second law of thermodynamics, there must be extra work to block the crack propagation in the traditional way. As reported, deformation work of UPBNNF cannot lead the different fracture mode of WC (Li et al., 2020). Combining mentioned analysis on UPBNNF, the probable reason is extra elastic work in the process of crack propagation of Si_3N_4 grains containing UPBNNF. The source of the elastic work cannot be found in the microstructure scale. Therefore, atomic theory is necessary when the fracture mode of materials is concerned in this case. A simple theory is the cohesive strength model. In this model, fracture is determined based on the cohesive strength of atoms, which is proportional to Young's modulus (Lawn, 1993). The Si_3N_4 in a nanopore could possess higher cohesive strength as a result of being restrained by the nanopore based on the previously mentioned elevated Young's modulus of parts of Si_3N_4. Thus, the fracture mode of Si_3N_4 in the composites with UPBNNF is consistent with an increase in Young's modulus. Young's modulus and fracture at the atomic scale are both the variations in force and distance between atoms (Lawn, 1993; Hsieh and Tuan, 2005).

As shown in results, one unusual observation is that the Young's modulus of the composites was even higher than the highest value, which is rarely present in other composites regardless of whether the second phase exists as a particle or fiber. Examples of these types of composites include Si_3N_4-*SiC*, Si_3N_4-TiN, Si_3N_4-ZrO_2, TaC-TaB_2, and ZrB_2-TiC (Akimune, 1990; Pezzotti, 1993; Blugan et al., 2005; Zhang et al., 2008; Guicciardi et al., 2010; Bódis et al., 2017). It is known that Young's modulus of materials as an intrinsic property is determined by the bonding between the individual atoms, which means Young's modulus is a characterization of force and distance between atoms (Meyors and Chawla, 1999). For materials containing pores, Young's modulus descends with higher porosity (Pabst and Gregorová, 2004). On evaluating Young's modulus of composites, the mixture rule is usually applied, and the value is located between the high and low values regardless of the calculation methods (Meyors and Chawla, 1999; Hsieh and Tuan, 2005). In addition, different methods are also applied to obtain this value. However, results derived from the examination methods or calculated by the mixture rule show only minimal differences. Therefore, all

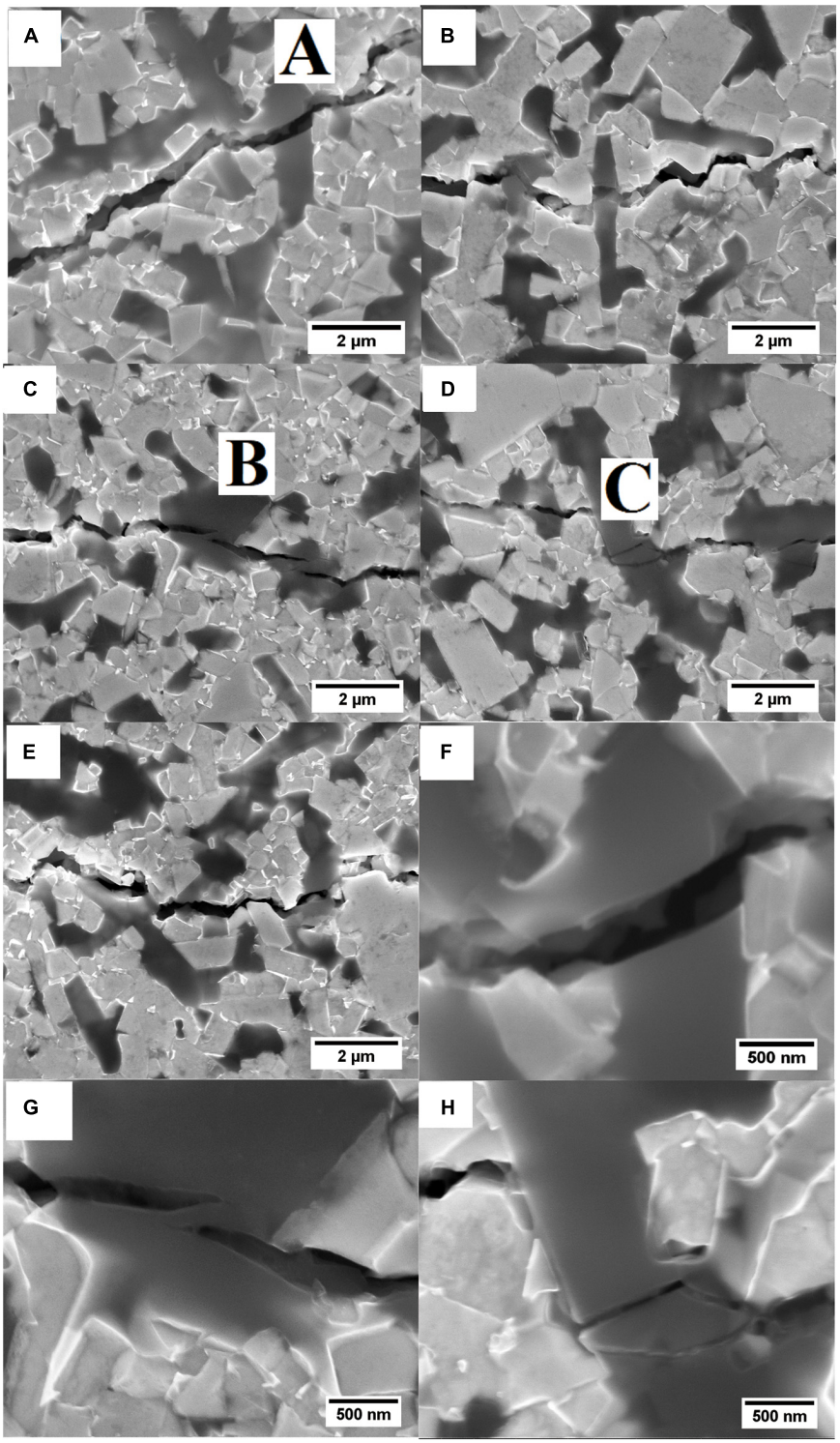

FIGURE 5 | HRSEM images of the indentation crack paths in of **(A)** 10S, **(B)** 10S0.01B, **(C)** 10S0.05B, **(D)** 10S0.1B, **(E)** 10S0.15B, **(F)** A area in **(A)**, **(G)** B area in **(C)**, and **(H)** C area in **(D)**.

methods are adopted in materials investigations (Koopman et al., 2002; Cha et al., 2003; Basu et al., 2004; Wang et al., 2012; Xia et al., 2020). In brief, the addition of a phase with a low Young's modulus leads to decreasing value of composites. UPBNNF possesses two features that result in negligible Young's modulus in WC-Si_3N_4 composites: high porosity and a turbostratic

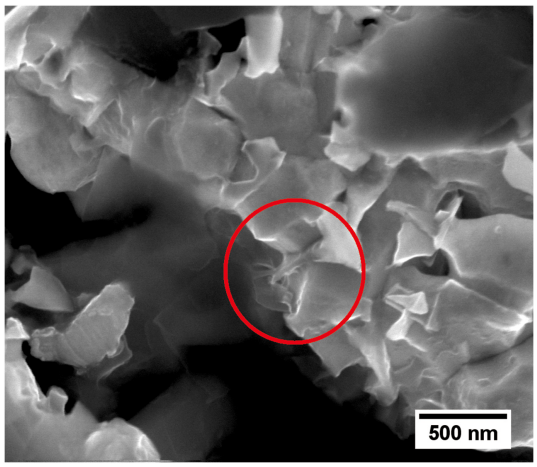

FIGURE 6 | Elongated Si_3N_4 grain pinned by UPBNNF in WC matrix.

structure that is related to a low Young's modulus of high tensile strength (HT) carbon fiber (Frank et al., 2012; Lin et al., 2016). In fact, the value of a BN fiber with a normal structure is only tens of GPa (Economy and Anderson, 1967). Therefore, the Young's modulus of UPBNNF itself has no effect on the composites. The only probable explanation is based on the most fundamental mechanism whereby the bonding of atoms is affected.

Meanwhile, there is no increase of Young's modulus found in WC-UPBNNF composites (Li et al., 2020). Young's modulus of some WC composites reported in published papers are listed in **Table 2**, which were all tested by the pulse-echo overlap ultrasonic technique. There are no abnormal phenomena, too. Thus, we consider that in addition to the liquid phase in the Si_3N_4 sintering process, the major point of influence is the nanosized pores of UPBNNF. For nanocrystalline materials (grain size < 50 nm), the properties could be modified at an atomic scale, but most of the modification is employed on functional ceramics (Gleiter, 1989; Jin and Bao, 1996; Maglia et al., 2013). It is rarely observed that Young's modulus of ceramics can be modified to increase thereafter, as no effective means are available to intervene at the atomic scale. Restricting the sizes of grains to less than 50 nm during the sintering process is difficult. However, it is possible that the bonding of atoms of Si_3N_4 can be affected after sintering by the presence of UPBNNF. As reported in the papers about WC-Si_3N_4 materials (Li et al., 2013; Zheng et al., 2013a, 2015), a liquid phase is generated during sintering, and then pores of UPBNNF can be filled with the liquid phase. In fact, reordering happened on groups of atoms in liquid phase sintering, and some groups were trapped in nanopores of UPBNNF. The bonding of atoms of Si_3N_4 in a pore is restrained after sintering, which means that the force and distance between atoms are also restricted. As a result, the Young's modulus of parts of Si_3N_4 increases, and in turn the values of whole Si_3N_4 and composites increase. Because of agglomeration, excess fraction of the fiber results in another decrease in Young's modulus. By contrast, directly observing the phenomenon is difficult. Regarding interaction between nanopores and filler materials, numerical modeling is mostly used. Even though accurate observation is employed on nanopores, there are too many requirements on the specimen itself (Lee et al., 2018; Gu et al., 2019; Hou et al., 2019; Nehra et al., 2019). WC-Si_3N_4 bulks after ball milling and sintering are too crude to meet the requirements. In addition, although some BN phases like BN nanoplates observed were reported (Ahmadi et al., 2017; Germi et al., 2018; Mahaseni et al., 2018), the turbostratic structure and pore leading to bad contrast hindered the intention of observation for UPBNNF in this case.

Eventually, synergic toughening is evident on the WC matrix, which is based on toughened Si_3N_4 and UPBNNF, as shown in **Figure 6**. By contrast, the synergic mechanism is not consistent with traditional ceramic-ceramic toughening theory. According to the traditional toughening model, weak interfacial bonding between non-binder second phases and the matrix is beneficial due to the fragile second phases without toughening effects in complex stress environments (Mahaseni et al., 2018). Energy is consumed by debonding, interfacial friction, and so on. In brief, energy must be consumed by generating new interfaces, but must not be alongside main cracks. Why the synergetic toughening is possible in this study? It was observed that Si_3N_4 is strongly bonded to the matrix by UPBNNF, so do UPBNNF itself. As a result, debonding between WC matrix and Si_3N_4 was more difficult, and the energy had to be consumed in other approaches like Si_3N_4 fracture. Usually, fracture in the ceramic second phase does not have considerable attribution to the toughening matrix due to the transitory nature of the fracture (Germi et al., 2018). However, as observed and elucidated, the ultimate fracture of Si_3N_4 grain in the composites can occur during a certain time interval. The aforementioned effects may consume more energy than traditional methods that lead to toughening.

The following is a brief summary of the previous discussion. First, it is possible that Young's modulus of ceramics is elevated using nanopores. High specific stiffness, which is a ratio of

TABLE 2 | Young's modulus of some WC composites reported in published papers.

Specimen	**0**[a]	**6Co**[b]	**1CNT**[c]	**6ZrO_2**[b]	**8ZrO_2**[d]	**1Si_3N_4**[e]	**3Si_3N_4**[e]	**6Si_3N_4**[e]	**8Si_3N_4**[e]
Young's modulus	704	649	658	575	559	650	596	542	522
Specimen	**10Si_3N_4**[e]	**12Si_3N_4**[e]	**15Si_3N_4**[e]	**0.05UPBNNF**[a]	**0.075UPBNNF**[a]	**0.1UPBNNF**[a]	**0.125UPBNNF**[a]		
Young's modulus	517	486	470	684	666	642	630		

The specimens' names are in terms of second phases with weight fraction in WC matrix.
Data sources: a, Li et al., 2020; b, Basu et al., 2004; c, Cao et al., 2018; d, Cao et al., 2021; e, Zheng et al., 2015.

Young's modulus to density, is often desired in mechanical design. However, the rule of mixture is a theoretical limitation, and no elevation exists beyond the intrinsic properties of materials that are simply affected at the atomic scale. Materials with high Young's modulus usually have a high density and result in increasing density after the addition into the matrix of a low Young's modulus. Second, ceramics with an internal liquid phase during sintering such as Si_3N_4 can employ a different fracture mode at the micrometer scale. Although no ductility can occur on the ceramics, serial and multiple fractures during a certain time interval may be closed to ductility in analogy with series approximation to a smooth function in calculus. Finally, a fiber with a deformation ability and modified ceramic phase such as those of the aforementioned Si_3N_4 enables the toughening of other ceramics jointly.

CONCLUSION

In this study, WC-10 wt.% Si_3N_4-x ($x = 0$, 0.01, 0.05, 0.1, and 0.15) wt.% UPBNNF composites were prepared by SPS. The following conclusions were drawn and thus present a means of improving the mechanical properties of ceramics.

(1) The addition of UPBNNF to WC-10 wt.% Si_3N_4 could be effective at enhancing hardness and maintaining fracture toughness.
(2) Tears and scratches patterns appear on Si_3N_4 grains in indentation crack paths of WC-Si_3N_4 composites with the addition of UPBNNF, an observation that is different from that of the traditional fracture mode of Si_3N_4 in which a catastrophic fracture occurs with clean edges.
(3) A collaborative toughening effect of UPBNNF and Si_3N_4 in WC-Si_3N_4 composites works under strong interfacial bonding.

DATA AVAILABILITY STATEMENT

The datasets generated for this study are available on request to the corresponding author.

AUTHOR CONTRIBUTIONS

TC: idea conceiving and writing. XL: supervising and project leader. SQ: supervising on mechanical tests. JL: assistant on preparing composites. LL: providing hardness tester. YH: supervising on porous fiber preparing. TS: preparing porous fiber. All authors contributed to the article and approved the submitted version.

FUNDING

This study was supported by the National Natural Science Foundation of China (Nos. 51474108, 51575193, and 51402086), the Hundred Talents Program of Hebei Province (E2014100011), the Key Project of Guangdong Natural Science Foundation (No. 2018B030311051), and the Heyuan Science and Technology Project (heke2018009).

REFERENCES

Ahmadi, Z., Nayebi, B., Asl, M. S., Kakroudi, M. G., and Farahbakhsh, I. (2017). Sintering behavior of ZrB_2-SiC composites doped with Si_3N_4: a fractographical approach. *Ceram. Int.* 43, 9699–9708. doi: 10.1016/j.ceramint.2017.04.144

Akimune, Y. (1990). Impact damage and strength degradation in a silicon carbide reinforced silicon nitride composite. *J. Am. Ceram. Soc.* 73, 3019–3025. doi: 10.1111/j.1151-2916.1990.tb06710.x

Anstis, G. R., Chantikul, P., Lawn, B. R., and Marshall, D. B. (1981). A critical evaluation of indentation techniques for measuring fracture toughness: I, direct crack measurements. *J. Am. Ceram. Soc.* 64, 533–538. doi: 10.1111/j.1151-2916.1981.tb10320.x

Basu, B., Lee, J. H., and Kim, D. Y. (2004). Development of WC-ZrO_2 nanocomposites by spark plasma sintering. *J. Am. Ceram. Soc.* 87, 317–319.

Becher, P. F. (1991). Microstructural design of toughened ceramics. *J. Am. Ceram. Soc.* 74, 25–69.

Becher, P. F., Hsueh, C. H., Angelini, P., and Tiegs, T. N. (1988). Toughening behavior in whisker-reinforced ceramic matrix composites. *J. Am. Ceram. Soc.* 71, 1050–1061. doi: 10.1111/j.1151-2916.1988.tb05791.x

Blugan, G., Hadad, M., Janczak-Rusch, J., Kuebler, J., and Graule, T. (2005). Fractography, mechanical properties, and microstructure of commercial silicon nitride-titanium nitride composites. *J. Am. Ceram. Soc.* 88, 926–933. doi: 10.1111/j.1551-2916.2005.00186.x

Bódis, E., Molnár, K., Mucsi, A., Károly, Z., Móczó, J., Klébert, S., et al. (2017). Silicon nitride-based composites reinforced with zirconia nanofibers. *Ceram. Int.* 43, 16811–16818. doi: 10.1016/j.ceramint.2017.09.078

Cao, T., Li, X., Li, J., Zhang, M., and Qiu, H. (2018). Effect of sintering temperature on phase constitution and mechanical properties of WC-1.0 wt.% carbon nanotube composites. *Ceram. Int.* 44, 164–169. doi: 10.1016/j.ceramint.2017.09.154

Cao, T., Li, X., and Li, J. (2021). Improvements of mechanical properties of WC-ZrO_2 composites with addition of ultrafine porous boron nitride nanofiber. *Rare Metal Mat. Eng.* 50, 802–806.

Cha, S. I., Hong, S. H., and Kim, B. K. (2003). Spark plasma sintering behavior of nanocrystalline WC-10Co cemented carbide powder. *Mater. Sci. Eng. A* 351, 31–38. doi: 10.1016/s0921-5093(02)00605-6

Chang, S. H., Chang, M. H., and Huang, H. T. (2015). Study on the sintered characteristics and properties of nanostructured WC-15 wt% (Fe-Ni-Co) and WC-15 wt% Co hard metal alloys. *J. Alloy Compd.* 649, 89–95. doi: 10.1016/j.jallcom.2015.07.119

Economy, J., and Anderson, R. V. (1967). Boron nitride fibers. *J. Polym. Sci. C.* 19, 283–297.

El-Eskandarany, M. S. (2000). Fabrication of nanocrystalline WC and nanocomposite WC-MgO refractory materials at room temperature. *J. Alloy Compd.* 296, 175–182. doi: 10.1016/s0925-8388(99)00508-3

El-Eskandarany, M. S. (2005). Fabrication and characterizations of new nanocomposite WC/Al_2O_3 materials by room temperature ball milling and subsequent consolidation. *J. Alloy Compd.* 391, 228–235. doi: 10.1016/j.jallcom.2004.08.064

Fattahi, M., Asl, M. S., Delbari, S. A., Namini, A. S., Ahmadi, Z., and Mohammadi, M. (2020a). Role of nano-WC addition on microstructural, mechanical and thermal characteristics of TiC-SiC_w composites. *Int. J. Refract. Met. Hard Mater.* 90:105248. doi: 10.1016/j.ijrmhm.2020.105248

Fattahi, M., Delbari, S. A., Babapoor, A., Namini, A. S., Mohammadi, M., and Asl, M. S. (2020b). Triplet carbide composites of TiC, WC, and SiC. *Ceram Int.* 46, 9070–9078. doi: 10.1016/j.ceramint.2019.12.155

Frank, E., Hermanutz, F., and Buchmeiser, M. R. (2012). Carbon fibers: precursors, manufacturing, and properties. *Macromol. Mater. Eng.* 297, 493–501. doi: 10.1002/mame.201100406

Germi, M. D., Mahaseni, Z. H., Ahmadi, Z., and Asl, M. S. (2018). Phase evolution during spark plasma sintering of novel Si_3N_4-doped TiB_2-SiC composite. *Mater. Charact.* 145, 225–232. doi: 10.1016/j.matchar.2018.08.043

Gleiter, H. (1989). Nanocrystalline materials. *Prog. Mater. Sci.* 33, 223–315.

Golberg, D., Bando, Y., Huang, Y., Terao, T., Mitome, M., Tang, C., et al. (2010). Boron nitride nanotubes and nanosheets. *ACS Nano* 4, 2979–2993.

Golberg, D., Bando, Y., Tang, C., and Zhi, C. (2007). Boron nitride nanotubes. *Adv. Mater.* 19, 2413–2432.

Gu, C., Lu, Y., Ridgeway, C. D., Cinkilic, E., and Luo, A. A. (2019). Three-dimensional cellular automaton simulation of coupled hydrogen porosity and microstructure during solidification of ternary aluminum alloys. *Sci. Rep.* 9:13099.

Guicciardi, S., Silvestroni, L., Nygren, M., and Sciti, D. (2010). Microstructure and toughening mechanisms in spark plasma-sintered ZrB_2 ceramics reinforced by SiC whiskers or SiC-chopped fibers. *J. Am. Ceram. Soc.* 93, 2384–2391. doi: 10.1111/j.1551-2916.2010.03730.x

Han, D., Mei, H., Xiao, S., Dassios, K. G., and Cheng, L. (2018). A review on the processing technologies of carbon nanotube/silicon carbide composites. *J. Eur. Ceram. Soc.* 38, 3695–3708. doi: 10.1016/j.jeurceramsoc.2018.04.033

Hou, J., Kong, X. S., Wu, X., Song, J., and Liu, C. S. (2019). Predictive model of hydrogen trapping and bubbling in nanovoids in bcc materials. *Nat. Mater.* 18, 833–839. doi: 10.1038/s41563-019-0422-4

Hsieh, C. L., and Tuan, W. H. (2005). Elastic properties of ceramic-metal particulate composites. *Mater. Sci. Eng. A* 393, 133–139. doi: 10.1016/j.msea.2004.10.009

Hu, Y., Chen, Z., Zhang, J., Xiao, G., Yi, M., Zhang, W., et al. (2019). Preparation and mechanical properties of Si_3N_4 nanocomposites reinforced by Si_3N_4@rGO particles. *J. Am. Ceram. Soc.* 102, 6991–7002. doi: 10.1111/jace.16546

Ii, S., Iwamoto, C., Matsunaga, K., Yamamoto, T., Yoshiya, M., and Ikuhara, Y. (2004). Direct observation of intergranular cracks in sintered silicon nitride. *Phil. Mag.* 84, 2767–2775. doi: 10.1080/14786430410001671485

Jin, H., Meng, S., Xie, W., Xu, C., and Niu, J. (2017). HfB_2-CNTs composites with enhanced mechanical properties prepared by spark plasma sintering. *Ceram. Int.* 43, 2170–2173. doi: 10.1016/j.ceramint.2016.10.200

Jin, Z., and Bao, Y. (1996). *Characterization of Mechanical Properties for Brittle Materials and Ceramics*. Beijing: China Railways Publishing House, 166–168.

Kim, H. C., Kim, D. K., Woo, K. D., Ko, I. Y., and Shon, I. J. (2008). Consolidation of binderless WC-TiC by high frequency induction heating sintering. *Int. J. Refract. Met. Hard. Mater.* 26, 48–54. doi: 10.1016/j.ijrmhm.2007.01.006

Klemm, H. (2010). Silicon nitride for high-temperature applications. *J. Am. Ceram. Soc.* 93, 1501–1522. doi: 10.1111/j.1551-2916.2010.03839.x

Koopman, M., Chawla, K. K., Coffin, C., Patterson, B. R., Deng, X., Patel, B. V., et al. (2002). Determination of elastic constants in WC/Co metal matrix composites by resonant ultrasound spectroscopy and impulse excitation. *Adv. Eng. Mater.* 4, 37–42. doi: 10.1002/1527-2648(20020212)4:1/2<37::aid-adem37>3.0.co;2-n

Kumar, A. K. N., Watabe, N., and Kurokawa, K. (2011). The sintering kinetics of ultrafine tungsten carbide powder. *Ceram. Int.* 37, 2643–2654. doi: 10.1016/j.ceramint.2011.04.011

Lawn, B. R. (1993). *Fracture of Brittle Solids, 2nd Version*. New York, NY: Cambridge University Press, 144–147.

Lee, K., Park, K. B., Kim, H. J., Yu, J. S., Chae, H., Kim, H. M., et al. (2018). Recent progress in solid-state nanopores. *Adv. Mater.* 30:1704680. doi: 10.1002/adma.201704680

Li, T., Chen, Y., Li, W., Li, J., Luo, L., Yang, T., et al. (2018). Fabrication and mechanical properties of boron nitride nanotube reinforced silicon nitride ceramics. *Ceram. Int.* 44, 6456–6460. doi: 10.1016/j.ceramint.2018.01.041

Li, X., Cao, T., Zhang, M., Qiu, H., Huang, Y., Qu, S., et al. (2020). Ultrafine porous boron nitride nanofiber-toughened WC composites. *Int. J. Appl. Ceram. Technol.* 17, 941–948. doi: 10.1111/ijac.13466

Li, Y., Zheng, D., Li, X., Qu, S., and Yang, C. (2013). Cr_3C_2 and VC doped WC-Si_3N_4 composites prepared by spark plasma sintering. *Int. J. Refract. Met. Hard. Mater.* 41, 540–546. doi: 10.1016/j.ijrmhm.2013.07.004

Lin, J., Xu, L., Huang, Y., Li, J., Wang, W., Feng, C., et al. (2016). Ultrafine porous boron nitride nanofibers synthesized via a freeze-drying and pyrolysis process and their adsorption properties. *RSC Adv.* 6, 1253–1259. doi: 10.1039/c5ra23426c

Maglia, F., Tredici, I. G., and Anselmi-Tamburini, U. (2013). Densification and properties of bulk nanocrystalline functional ceramics with grain size below 50 nm. *J. Eur. Ceram. Soc.* 33, 1045–1066. doi: 10.1016/j.jeurceramsoc.2012.12.004

Mahaseni, Z. H., Germi, M. D., Ahmadi, Z., and Asl, M. S. (2018). Microstructural investigation of spark plasma sintered TiB2 ceramics with Si_3N_4 addition. *Ceram. Int.* 44, 13367–13372. doi: 10.1016/j.ceramint.2018.04.171

Marshall, D. B., and Evans, A. G. (1985). Failure mechanisms in ceramic-fiber/ceramic-matrix composites. *J. Am. Ceram. Soc.* 68, 225–231. doi: 10.1111/j.1151-2916.1985.tb15313.x

Meyors, M. A., and Chawla, K. K. (1999). *Mechanical Behavior of Materials, 2nd Version*. New York, NY: Cambridge University Press.

Namini, A. S., Ahmadi, Z., Babapoor, A., Shokouhimehr, M., and Asl, M. S. (2019). Microstructure and thermomechanical characteristics of spark plasma sintered TiC Ceramics doped with nano-sized WC. *Ceram. Int.* 45, 2153–2160. doi: 10.1016/j.ceramint.2018.10.125

Nehra, A., Ahlawat, S., and Singh, K. P. (2019). A biosensing expedition of nanopore: a review. *Sens. Actuator B Chem.* 284, 595–622. doi: 10.1016/j.snb.2018.12.143

Nino, A., Izu, Y., Sekine, T., Sugiyama, S., and Taimatsu, H. (2019). Effects of TaC and TiC addition on the microstructures and mechanical properties of binderless WC. *Int. J. Refract. Met. Hard. Mater.* 82, 167–173. doi: 10.1016/j.ijrmhm.2019.04.012

Norgren, S., García, J., Blomqvist, A., and Yin, L. (2015). Trends in the P/M hard meal industry. *Int. J. Refract. Met. Hard. Mater.* 48, 31–45. doi: 10.1016/j.ijrmhm.2014.07.007

Pabst, W., and Gregorová, E. (2004). New relation for the porosity dependence of the effective tensile modulus of brittle materials. *J. Mater. Sci.* 39, 3501–3503. doi: 10.1023/b:jmsc.0000026961.12735.2a

Pezzotti, G. (1993). Si_3N_4/SiC-platelet composite without sintering aids: a candidate for gas turbine engines. *J. Am. Ceram. Soc.* 76, 1313–1320. doi: 10.1111/j.1151-2916.1993.tb03757.x

Pigeon, R. G., and Varma, A. (1992). Quantitative phase analysis of Si_3N_4 by x-ray diffraction. *J. Mater. Sci. Lett.* 11, 1370–1372.

Poetschke, J., Richter, V., and Holke, R. (2012). Influence and effectivity of VC and Cr_3C_2 grain growth inhibitors on sintering of binderless tungsten carbide. *Int. J. Refract. Met. Hard. Mater.* 31, 218–223. doi: 10.1016/j.ijrmhm.2011.11.006

Riley, F. L. (2000). Silicon nitride and related materials. *J. Am. Ceram. Soc.* 83, 245–265. doi: 10.1111/j.1151-2916.2000.tb01182.x

Sakkaki, M., Moghanlou, F. S., Vajdi, M., Pishgar, F., Shokouhimehr, M., and Asl, M. S. (2019). The effect of thermal contact resistance on the temperature distribution in a WC made cutting tool. *Ceram. Int.* 45, 22196–22202. doi: 10.1016/j.ceramint.2019.07.241

Tatarko, P., Grasso, S., Porwal, H., Chlup, Z., Saggar, R., Dlouhý, I., et al. (2014). Boron nitride nanotubes as a reinforcement for brittle matrices. *J. Eur. Ceram. Soc.* 34, 3339–3349. doi: 10.1016/j.jeurceramsoc.2014.03.028

Vasudevan, S., Kothari, A., and Sheldon, B. W. (2016). Direct observation of toughening and R-curve behavior in carbon nanotube reinforced silicon nitride. *Scripta Mater.* 124, 112–116. doi: 10.1016/j.scriptamat.2016.06.035

Wang, B., Matsumaru, K., Yang, J., Fu, Z., and Ishizaki, K. (2012). The effect of cBN additions on densification, microstructure and properties of WC-Co composites by pulse electric current sintering. *J. Am. Ceram. Soc.* 95, 2499–2503. doi: 10.1111/j.1551-2916.2012.05218.x

Wang, W. L., Bi, J. Q., Sun, K. N., Du, M., Long, N. N., and Bai, Y. J. (2011). Fabrication of alumina ceramic reinforced with boron nitride nanotubes with improved mechanical properties. *J. Am. Ceram. Soc.* 94, 3636–3640. doi: 10.1111/j.1551-2916.2011.04821.x

Xia, C., Asl, M. S., Namini, A. S., Ahmadi, Z., Delbari, S. A., Le, Q. V., et al. (2020). Enhanced fracture toughness of ZrB_2-SiC_w ceramics with graphene nano-platelets. *Ceram. Int.* 46, 24906–24915. doi: 10.1016/j.ceramint.2020.06.275

Yadhukkulakrishnan, G. B., Rahman, A., Karumuri, S., Stackpoole, M. M., Kalkan, A. K., Singh, R. P., et al. (2012). Spark plasma sintering of silicon carbide and multi-walled carbon nanotube reinforced zirconium diboride ceramic composites. *Mater. Sci. Eng. A* 552, 125–133. doi: 10.1016/j.msea.2012.05.020

Zhang, J., Zhang, G., Zhao, S., and Song, X. (2009). Binder-free WC bulk synthesized by spark plasma sintering. *J. Alloy Compd.* 479, 427–431. doi: 10.1016/j.jallcom.2008.12.151

Zhang, X., Hilmas, G. E., and Farenholtz (2008). Densification, mechanical properties, and oxidation resistance of TaC-TaB2 ceramics. *J. Am. Ceram. Soc.* 91, 4129–4132. doi: 10.1111/j.1551-2916.2008.02780.x

Zheng, D., Li, X., Ai, X., Yang, C., and Li, Y. (2012). Bulk WC-Al_2O_3 composites prepared by spark plasma sintering. *Int. J. Refract. Met. Hard. Mater.* 30, 51–56.

Zheng, D., Li, X., Li, Y., Qu, S., and Yang, C. (2013a). In-situ elongated β-Si_3N_4 grains toughened WC composites prepared by one/two-step spark plasma sintering. *Mater. Sci. Eng. A* 561, 445–451. doi: 10.1016/j.msea.2012.10.059

Zheng, D., Li, X., Li, Y., Qu, S., and Yang, C. (2013b). ZrO_2 (3Y) toughened WC composites prepared by spark plasma sintering. *J. Alloy Compd.* 572, 62–67. doi: 10.1016/j.jallcom.2013.03.259

Zheng, D., Li, X., Tang, Y., and Cao, T. W. C. - (2015). Si_3N_4 composites prepared by two-step spark plasma sintering. *Int. J. Refract. Met. Hard. Mater.* 50, 133–139.

Zhou, Y., Ohji, T., Hyuga, H., Yoshizawa, Y., Murayama, N., and Hirao, K. (2014). Fracture resistance behavior of high-thermal-conductivity silicon nitride ceramics. *Int. J. Appl. Ceram. Technol.* 11, 872–882. doi: 10.1111/ijac.12109

Conflict of Interest: The authors declare that the research was conducted in the absence of any commercial or financial relationships that could be construed as a potential conflict of interest.

The reviewer ZW declared a shared affiliation, with no collaboration, with several of the authors, TC, XL, JL, SQ, and LL, to the handling editor at the time of the review.